Journal of Catalysis 267 (2009) 158–166

Contents lists available at ScienceDirect

Journal of Catalysis

journal homepage: www.elsevier.com/locate/jcat

Investigation of the selective sites on graphitic carbons for oxidative dehydrogenation of isobutane

Hong Xie, Zili Wu, Steven H. Overbury, Chengdu Liang *, Viviane Schwartz *

Center for Nanophase Materials Sciences, Oak Ridge National Laboratory, Oak Ridge, TN 37831, USA

ARTICLE INFO

Article history:
Received 26 June 2009
Revised 10 August 2009
Accepted 10 August 2009
Available online 10 September 2009

Keywords:
Carbon catalysts
Oxidative dehydrogenation
Isobutane
Isobutene
Graphitized mesoporous carbon
Edge sites
Quinone sites

ABSTRACT

Reaction network analysis of the oxidative dehydrogenation (ODH) reaction of isobutane over model carbon catalysts with tailored open-edge graphitic structure and quinone-type oxygenated functionalities was used to identify the selective pathways for the formation of isobutene. Carbon-based materials have been widely used in catalysis, but the active sites are not well-understood due to the complexity of the carbon structure. Correct identification of these sites is essential for learning how to manipulate material structure to achieve high catalytic yields of the desired products. In this study, we created model catalysts with controllable surface concentration of oxygen based on graphitized mesoporous carbon (GMC). Our studies reveal that the ODH reaction of isobutane on carbon catalysts is a parallel-consecutive pathway with partial oxidative dehydrogenation for the formation of isobutene and deep oxidation pathway for the direct formation of CO and CO_2 from isobutane. These two pathways show different dependence on the quinone-type oxygen sites: the rate constant leading to the desired partial oxidation product does not show a strong correlation to the density of the oxygen sites, whereas the rate constant leading to the unselective CO_x products increases continuously with the density of oxygen sites.

1. Introduction

Isobutene is the most versatile chemical intermediate among all C_4 olefins. The demand for isobutene has been increasing continuously over the years due to its importance as a monomer in the synthesis of various organic products for chemical and polymer industries. Conventional dehydrogenation route using metal catalysts for light olefin synthesis usually involves a high temperature endothermic process which has several disadvantages such as catalyst deactivation by coke formation and the consequent need for periodic catalyst regeneration [1]. Alternatively, oxidative dehydrogenation (ODH) reaction of paraffins to their corresponding olefins has received increasing attention since, as an exothermic process, ODH reaction requires much less energy consumption than dehydrogenation process which is commonly adopted in current industrial operations.

Most of the studies on ODH reactions have been done using transition metal oxide catalysts such as Mg–V–Sb-oxide, vanadium oxide, and manganese molybdate [1–3]. One of the major challenges of this kind of reaction is to be able to minimize the combustion side reactions leading to the undesired CO and CO_2 products while increasing the limited alkene selectivity achieved by these catalysts. The chemical complexity of the oxide catalysts leading to their activity can also be detrimental to the elucidation of the active sites responsible for high selectivity.

Carbon-based catalysts have proven to be attractive alternatives to the conventional metal-based ones. Carbon materials have significant advantages due to their unparalleled flexibility as their physical and chemical properties can be tailored for specific needs. So far, activated carbon, carbon nanofibers, and carbon nanotubes have been reported to catalyze ODH reactions with high selectivity results. Delgado et al. [4] reported catalytic activity of carbon nanofibers immobilized on carbon felt support for the ODH reaction of ethyl benzene. Díaz Velásquez et al. [5] tested the surface-modified activated carbon for the isobutane ODH reaction, and considered the carbonyl/quinone groups on the surface as the active sites, where the isobutene yields were lower with lower concentrations of these groups. Due to the diverse nature of the structure and functionalities present in different carbon materials including the traditional activated carbons and the carbon nanotubes, the active sites of ODH reactions on carbon materials leading to the formation of the desired unsaturated products still have not been clarified. The precise mechanism of the ODH reaction over carbon surface remains controversial due to undetermined metal impurities as found in activated carbons and carbon nanotubes, dangling bonds, mixed sp^2 and sp^3 hybridization, surface functional groups, and the defect/edge sites, which could all contribute to the reactivity with different selectivity.

* Corresponding authors.
E-mail addresses: liangcn@ornl.gov (C.D. Liang), schwartzv@ornl.gov (V. Schwartz).

0021-9517/$ - see front matter © 2009 Elsevier Inc. All rights reserved.
doi:10.1016/j.jcat.2009.08.005

In order to identify the active sites of the ODH reaction on carbon catalysts, model compounds have been used to simplify the catalytic system and thereby leading to better understanding of the catalytic properties of carbon catalysts. A recent publication by Zhang et al. [6] used surface-modified carbon nanotubes as model catalysts and discovered that the nature of the surface oxygen species has a strong correlation with the selectivity of the catalysts: electrophilic oxygen species (converted from oxygen molecules on the defect/edge sites) led to unselective total combustion of *n*-butane and nucleophilic-oxygenated groups led to the preferential ODH reaction that formed butaldiene. More recently, we demonstrated that the graphitized mesoporous carbon (GMC) with controllable openness of the graphite edge sites is an excellent model catalyst for the study of active sites in the ODH reaction on carbon catalysts [7]. The open graphitic edges in the GMC catalyst have been identified as the active sites for the ODH of isobutane. Interestingly, the initial existence of the oxygenated functional groups, mainly carbonyl groups, on the open graphitic edges of GMC catalyst shows no effect on its catalytic performance. The GMC catalysts with or without initial oxygen functional groups show negligible differences in the selectivity and reactivity. A plausible reason for this observation is that the open edge sites on the graphitic carbon are very active and the oxygenated functional groups are formed promptly when the reactant oxygen is introduced into the system. Indeed, oxygenated functional groups were observed after the ODH reaction even for the GMC catalyst without initially attached oxygenated groups. Although the edge sites are unambiguously the active sites for the ODH reaction, the role of the oxygenated functionalities that are either initially attached on the carbon catalysts surface or generated during the reaction has not been systematically studied on model catalysts. Revealing the role of these oxygenated functionalities in the ODH reaction is crucial for the fundamental understanding of the ODH reaction mechanism of hydrocarbons over carbon catalysts. Reaction kinetic analysis on carbon catalysts has been rarely studied, particularly on designed model catalysts. Therefore, a detailed kinetic study of the ODH reaction on model catalysts with intentionally generated functionalities will be valuable for gaining such a fundamental understanding of ODH reaction on carbon catalysts.

We report herein a detailed study on the reaction kinetics on carbon catalysts with tightly controlled surface functionality to gain insights on the reaction mechanism of ODH reactions. The GMC is an appealing model catalyst because of its simplicity in structure and surface functionality. In this study, we created synthetic carbon catalysts with controlled surface concentration of oxygenated functionalities based on GMC. These compounds have been investigated as model carbon catalysts for the ODH reaction of isobutane to reveal the reaction network at differential reaction conditions. We validate that the ODH reaction on carbon catalysts is a multistep parallel-sequential reaction path which has been thoroughly demonstrated over oxide catalysts [1,3,8,9]. Furthermore, the derived reaction rate constants for each step clarified the factors leading to superior selectivity to isobutene on these model carbon catalysts.

2. Experimental

2.1. Synthesis of model catalysts

Pluronic surfactant F127, phloroglucinol, hydrochloric acid (37 wt%), and formaldehyde (37 wt%) were obtained from Sigma–Aldrich, and anhydrous ethanol was purchased from Pharmco Aaper. The preparation of mesoporous carbon precursors was carried out following a procedure established by our group [7,10]. Briefly, F127 (50.4 g), phloroglucinol (25.2 g), and hydrochloric acid 37 wt% aqueous solution (10.0 g) were mixed in an round-bottomed flask and dissolved in 1300 ml of anhydrous ethanol. The resulting mixture was then heated with vigorous stirring until reflux. An aqueous solution of 26.0 g of formaldehyde 37 wt% was added to the reaction mixture. The heating and stirring were continued for additional 2 h. Orange-colored particles were collected after the reaction and were further pyrolysized at 850 °C in a tube furnace (Thermolyne, model: 79300) in the presence of nitrogen. The resulting carbon materials were then treated in helium at 2600 °C in a graphite furnace (Thermal Technologies, model: 1000-2560-FP20) to reach the starting material of pristine graphitic mesoporous carbon denoted as sample SK0.

In our previous study we found out that our GMC pristine precursor can be homogeneously oxidized by air at 500 °C [7]. At this condition, we ensured the integrity of the graphitic structure while opening the fullerene-like cavities and creating open edges on its structure. Additionally, oxygen functional groups were created during the oxidation in air. In this study, the burn-off (B.O.) level, defined as the weight loss percentage after the oxygen treatment, and the amount of oxygenated groups were systematically varied by changing the duration of the oxidation treatment. The GMC samples prepared by this systematic approach were labeled as SK1, SK2, SK3, and SK4 corresponding to the oxidation treatment of 24 h, 30 h, 36 h, and 48 h, respectively.

2.2. Characterization of the physical structure of GMC catalysts

The nanometer-sized graphite crystals were characterized by Raman spectra, which were collected via fiber optics connected directly to the spectrographic stage of a triple spectrometer (Princeton Instruments Acton Trivista 555). Edge filter (Semrock) was used in front of the UV–Vis fiber optic bundle (Princeton Instruments) to block the laser irradiation. The 532 nm excitation was emitted from a solid state laser (Princeton Scientific, MSL 532-50) and the power was about 20 mW at the sample. The sample sat on a XY stage (Prior Scientific, OptiScan XY system) and translated in raster mode while collecting the spectrum in order to eliminate/minimize any laser damage of the samples. Cyclohexane solution was used as a standard for the calibration of the Raman shifts.

The porous structures of the model catalysts were characterized by physisorption. N_2 adsorption and desorption isotherms were measured in liquid N_2 at 77 K using an AUTOSORB-1C instrument (Quantachrome Corporation, USA). The samples were outgassed at 200 °C for 2 h prior to the isotherm measurement. The Brunauer–Emmett–Teller (BET) specific area, S_{BET}, was calculated from the relative pressure $0.05 < \frac{P}{P_0} < 0.3$ interval; and the total pore volume, V_{total}, at $\frac{P}{P_0} = 0.95$. The pore size distribution was calculated based on Barrett–Joyner–Halender (BJH) method using $0.05 < \frac{P}{P_0} < 0.94$ interval of the adsorption branch of the isotherm.

2.3. Probing surface functionalities

The surface-oxygenated functionalities before and after reaction were characterized by Temperature-Programmed Desorption (TPD) using a U-tube reactor (Altamira AMI-200) in flowing helium (20 ml/min) with a heating rate of 10 K/min from 298 K to 1300 K. The amounts of CO and CO_2 desorbed were quantified by a quadrupole mass spectrometer equipped with a 1 m long gas sampling capillary (Pfeiffer-Balzer Omnistar).

2.4. Catalytic measurements

The catalytic performance test for isobutane ODH reaction was carried out at atmospheric pressure in a packed bed stainless steel autoclave reactor (PID Eng & Tech, Spain). The feed consisted of iso-

butane and oxygen at 2.02 and 1.01 kPa, respectively, with balance N_2. The gases 2% O_2 (balance N_2) and 4% i-C_4H_{10} (balance N_2) were purchased from Air Liquid.

An amount of 200 mg catalyst was used to yield a gas hourly space velocity (GHSV) of 5100 h^{-1}. The reaction temperature was set to 400 °C and controlled by a thermocouple located inside the reactor bed. The reactants and products were analyzed using an on-line gas chromatography conducted on an Agilent 6890N Gas Chromatography system with a Hayesep N column and a molecular sieve column. CO and CO_2 were converted to CH_4 through a methanizer before they passed through a flame ionization detector for analysis. Isobutene, CO, and CO_2 were the only products detected. In all tests, carbon mass balances were within 100 ± 1%.

The reaction network analysis was performed at differential reaction conditions. Two different sets of experiments were conducted at 400 °C: in the first set, for reaction rate dependence on O_2 partial pressure study, the isobutane partial pressure $(P_{i\text{-}C_4H_{10}})$ was kept at 0.45 kPa while the oxygen partial pressure (P_{O_2}) was varied to yield relative oxygen mole fraction $\left(\frac{P_{O_2}}{P_{O_2}+P_{i\text{-}C_4H_{10}}} \times 100\%\right)$ between 20% and 80%. In the second set, for initial reaction rate and selectivity study, $P_{i\text{-}C_4H_{10}}$ and P_{O_2} were kept constant at 2.02 and 1.01 kPa, respectively. Isobutane conversion was varied by changing the feed flow rate from 40 to 160 sccm with 200 mg of carbon catalyst. The reaction rate and selectivity were extrapolated to zero contact time in order to determine the rate constants of primary and secondary reactions. In all cases, the feed was diluted with N_2 and He, and the total isobutane conversion was controlled below 5% to ensure differential conditions.

3. Results and discussion

3.1. Structure of and functional groups on the GMC model catalysts

As we discovered in our previous research, the secondary porosity with a pore size of 2.4 nm in the GMC can be opened through air oxidation [7]. In this process, a portion of the carbon, most likely the defects on the GMC, is gasified. This gasification process results in open graphite edges that can be covered with oxygen-containing groups. These open edges are more active than the basal plane of the graphite; therefore, higher burn-off level continues the gasification of the edge sites and leads to the shrinking of graphite nanodomains in the a, b plane. Consequently, the L_a value, defined as the size of the a, b plane (basal plane), is expected to decrease in the GMC with high burn-off level. Tuinstra and Koening studied the size dependence of the graphite nanocrystals to the ratio of the D- and G-band intensities in the Raman spectrum of carbon [11]. The TK equation describes that the ratio of intensities of the D- to G-band is proportional to the inverse of L_a. The Raman spectra of the GMCs with various burn-off levels are shown in Fig. 1. The spectra are normalized to the G-band intensity to highlight the trend of the D-band intensity. Obviously, the D-band of the GMC increases with the increase of the burn-off level. Thus, the L_a value of the GMC decreases with the burn-off level. The gasification of the GMC is along the direction of the a, b plane, namely, the basal plane. This observation indicates that the ratio of the edge sites to the basal plane sites progressively increases with the oxidative gasification of the GMC. Increase of the edge sites with burn-off level is also validated by the work derived by Ferrari et al., [12] in which a relationship was found between the ratio of intensities of the D- to G-band and sp^3 content in amorphous carbon. In our previous study, we found that the basal plane is inert for ODH reaction; and the surface oxygen is attached to the edge plane. Hence, the oxidation of GMC with controlled burn-off level could possibly generate surface oxygen at continuously adjustable concentration on the edge surface of GMC. Two additional conditions have to be met to validate the oxidative gasification as a method for the creation of functionalities on GMC in a controllable manner: (1) the integrity of the GMC should be conserved to ensure that the gasification does not cause the collapse of the porous structure; and (2) the nature of the surface oxygen (type of functionality) should be independent of the burn-off level of the GMC.

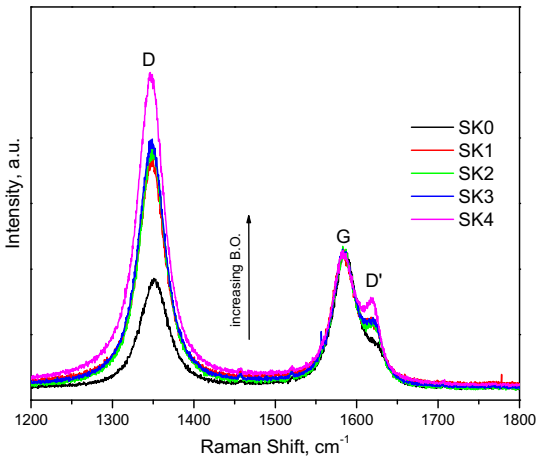

Fig. 1. Raman spectra of pristine GMC (SK0) and GMCs (SK1, SK2, SK3, and SK4) with increasing burn-off levels.

N_2 physisorption confirms that the structural integrity of the GMC is conserved with a burn-off level up to 70%. N_2 adsorption–desorption isotherms of GMCs are shown in Fig. 2. These isotherms are type IV isotherms with H1 hysteresis that corresponds to the uniform large mesopores formed through the polymer templates [7,10,13–15]. The specific surface area and pore volume of the GMCs with different burn-off levels are given in Table 1. A significant increase of the pore volume and surface area of SK1 was observed when the pristine GMC (SK0) was slightly oxidized. This abrupt increase of surface area and pore volume is mainly attributed to the opening of the voids in the fullerene-like cavities caused by oxidative pitting at the defect sites as discussed in our previous studies [7]. Further increase of the burn-off level gives a steady and less sharp increase in the surface area and pore volume of the GMCs due to the continuous decrease of the graphite nanocrystal size caused by the oxidative process. The decrease of the graphite nanocrystal size was verified in our previous work by X-ray diffraction [7]. The XRD patterns before and after gasification (not shown) presented similar features characteristic of graphitic

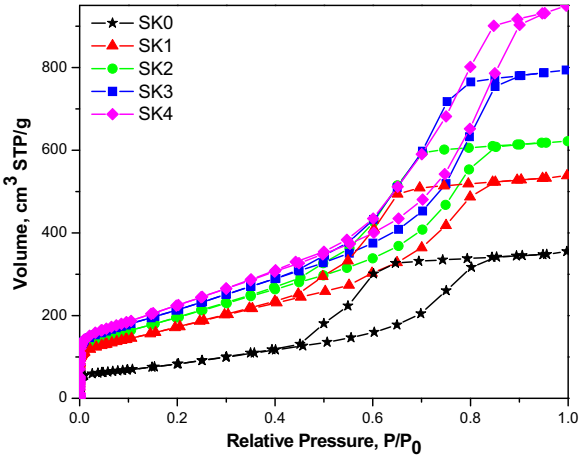

Fig. 2. N_2 adsorption–desorption isotherms for GMCs at 77 K.

Table 1
BET surface area and pore volume for GMCs.

GMC	B.O. (%)	S_{BET} (m^2/g)	V_{total} (cm^3/g)
SK0	0	311	0.54
SK1	13	629	0.83
SK2	20	717	0.96
SK3	33	784	1.22
SK4	70	832	1.44

material [7], confirming the integrity of the GMC structure throughout the oxidation process.

The pore size distributions of the GMCs (Fig. 3) further confirm that the oxidative gasification process, although destructive, has no effect on the integrity of the framework of the GMCs. All samples show bimodal distributions of mesopores with a lower peak centered at 2.4 nm for all carbons and a higher peak centered at about 7.6 nm for SK0 and SK1 carbons, 8.1 nm for SK2 carbon, and 8.8 nm for SK3 and SK4 carbons, respectively. While the small pores had a narrow distribution between 2.5 and 4.5 nm for all these carbons, the large pore size distribution became broader with increasing B.O. (Fig. 3), which suggests that further treatment in air for extended time at 500 °C slightly expands the large mesopores with less influence over the small mesopores in these carbons.

The surface oxygen functional groups were examined by TPD. The similar curve profiles of all the carbon catalysts suggest that the oxidation of the GMCs developed the same type of oxygenated functional groups on the surface of GMCs. While their surface concentration increases with the increase of the burn-off level, the composition of the oxygenated groups remains the same for all levels of burn-off. The CO desorption profile for the GMCs is shown in Fig. 4a. A pronounced peak at about 1023 K was observed, which can be associated to phenol, quinone or semiquinone groups formed on zig-zag edges [16–18]. Quinone-type surface groups have been reported as the active sites for ODH reaction [19]. For the CO_2 desorption shown in Fig. 4b, two pronounced peaks at about 548 K and 923 K were observed, which should correspond to the lactone groups [17]. In addition, a shoulder at ~833 K was also observed, which corresponds to anhydride groups [20]. No CO or CO_2 desorption from the untreated precursor material, SK0 carbon, was detected, which confirms a clean and inert surface for the pristine graphitic carbon.

Table 2 summarizes the amounts of CO and CO_2 species evolving from GMCs through TPD. The data show that the desorbed CO amount was one order of magnitude greater than that of CO_2 for all samples. The ratios CO/CO_2 were essentially constant for these four

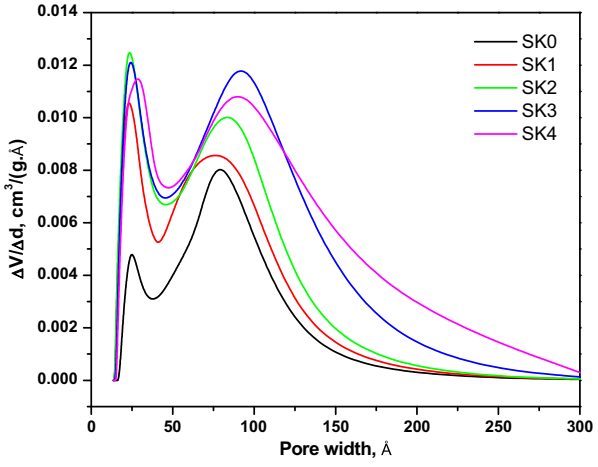

Fig. 3. Pore size distribution for SK0, SK1, SK2, SK3, and SK4 carbons.

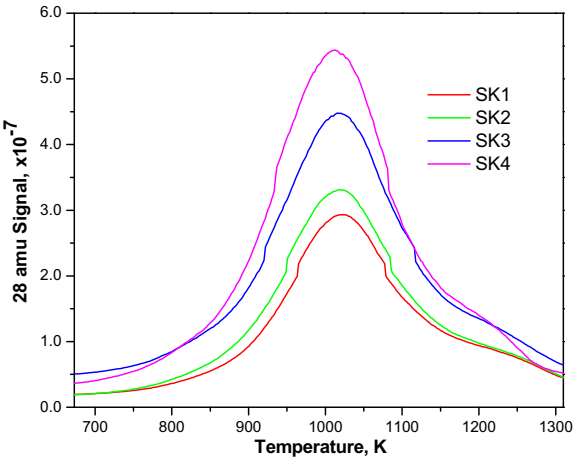

Fig. 4a. CO desorption spectra during TPD of fresh GMCs.

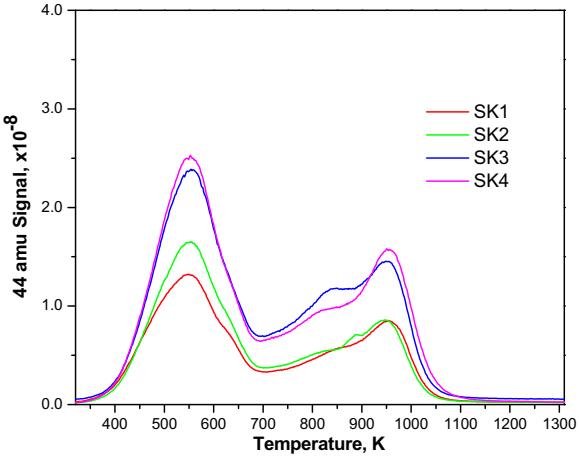

Fig. 4b. CO_2 desorption spectra during TPD of fresh GMCs.

Table 2
Calculated amounts of CO and CO_2 desorbed during TPD (N: μmol/g).

GMC	N_{CO}	N_{CO_2}	$\sum N_O$	N_{CO}/N_{CO_2}
SK1	923	96	1115	9.6
SK2	1129	107	1343	10.5
SK3	1534	174	1882	8.8
SK4	1901	180	2261	10.6
SK1[a]	752	70	892	10.8
SK2[a]	980	93	1166	10.5
SK3[a]	1129	114	1357	9.9
SK4[a]	1426	153	1731	9.3

[a] Used carbon after reaction.

carbons averaging around 9.9, corroborating that the distribution of surface-oxygenated functional groups is comparable on all GMCs. Similar trends were also observed for used carbon catalysts after ODH reaction (Figs. 5a and 5b); the ratios of CO/CO_2 stayed the same at around 9.9. The disappearance of the low temperature CO_2 desorption peak after reaction (Fig. 5b) is consistent with the fact that these carbons were exposed to a temperature of 400 °C during ODH tests. However, considering that the amount of CO_2 desorbed was an order of magnitude smaller compared to that of the CO, the contribution from these lactones to the ODH reaction should be secondary.

The amount of desorbed CO_x decreased about 20% for each carbon after reaction. This could be due to the formation of unstable

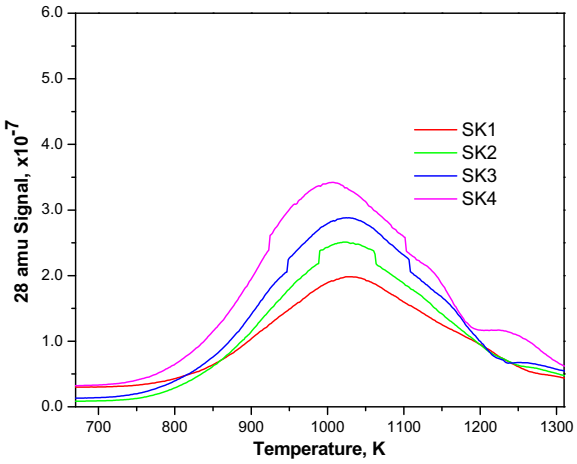

Fig. 5a. CO desorption spectra during TPD of used GMCs.

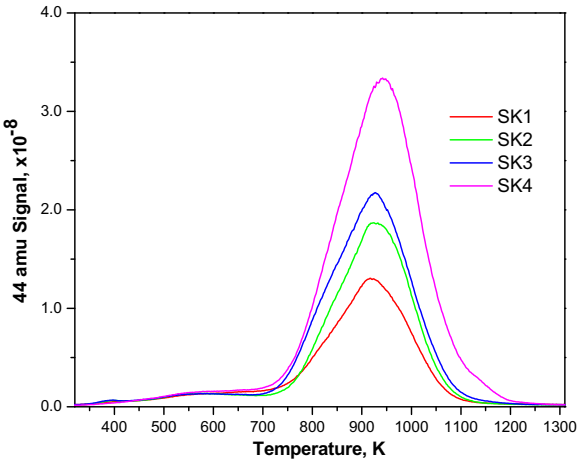

Fig. 5b. CO_2 desorption spectra during TPD of used GMCs.

O-containing surface groups on the carbons during the oxidation treatment, that desorbed in the presence of isobutane during reaction. It is also consistent with the observation that the reactivity of ODH of isobutane in the first 10 h showed a slightly higher reactivity before it reached steady-state as discussed below. Nevertheless, these GMCs had similar and well-developed surface oxygen-containing groups which were considerably stable during the course of ODH reaction.

The amount and the nature of the oxygen-containing surface functional groups can vary over a wide range, and both depend on the type of the oxidizing agent used, on the conditions of the modification process, and on the nature of the carbon precursor material. A variety of surface functional groups could be originated from the precursor material and it is particularly true in the case of carbons originated from oxygen-rich raw materials followed by incomplete carbonization [20,21]. In our case, the use of a highly pure carbon synthesized using an ultrahigh temperature process can be very advantageous as it narrows down significantly the range of possible functional groups present on the carbon surface that undergoes further oxidative treatment. Certainly, the assignment of the TPD peaks can be questionable as it is affected by many factors such as carbon texture, heating rate, and experimental set-up. However, by coupling our knowledge of the carbon material and the synthesis process with the observed CO and CO_2 peak temperature profiles, we can limit even further the possible oxygen-containing species being formed at the carbon surface. We conclude that mainly quinone-type groups should be forming at the surface based on the high temperature dry air oxidation process, the pristine nature of the carbon precursor, the peak temperature of CO elution, and the high value obtained for the CO/CO_2 ratio. Although phenol groups could also desorb as CO at the observed temperature range, the oxidation of GMC at 500 °C in dry air excludes the formation of functional groups containing hydroxyl groups since there was no source of hydrogen from the precursor synthetic carbon. Moreover, no H_2O desorption was detected. These quinone-type functional groups are continuously generated on the GMC surface at all burn-off levels. As confirmed by the Raman and physisorption measurements, these model catalysts share the same framework structure with differences in the ratio of the edge- to the basal-planes, which also results in the differences in the concentration of the oxygenated functionalities. Therefore, the controlled air oxidation of GMCs at 500 °C is a valid approach for the synthesis of model catalysts with tunable concentration of surface quinone-type functionalities.

3.2. Catalytic performance and reaction pathway

A blank gas phase homogeneous reaction of isobutane with O_2 was measured in the reactor packed with quartz beads and no conversion of isobutane was detected under reaction conditions confirming the absence of such homogeneous reaction. To verify the absence of mass transfer limitations, Thiele Modulus [22,23] were calculated and values significantly inferior to 0.4 were obtained, confirming the absence of mass transfer limitation on the mesoporous carbons under reaction conditions. Under the presence of the GMC catalysts, the main reaction products were isobutene, CO, and CO_2. Figs. 6 and 7 show comparisons of the specific rate of isobutane consumed and isobutene selectivity versus time-on-stream (TOS) for all the functionalized GMC catalysts, respectively. After a short period of slight deactivation, all the carbons reached steady-state and showed exceptional stability during 20 h of test. Similar initial deactivation behavior has also been observed elsewhere [5].

During the 20 h TOS, the isobutane conversion increased and the selectivity decreased with increasing B.O. level. The increase in overall isobutane conversion suggests that more active sites are available for GMCs with higher B.O. for the ODH reaction. The higher consumption rate of isobutane was accompanied by lower isobutene selectivity, which suggests a parallel-consecutive reaction network as will be discussed later. Both CO and CO_2 can be formed by deep oxidation of isobutane and isobutene, and

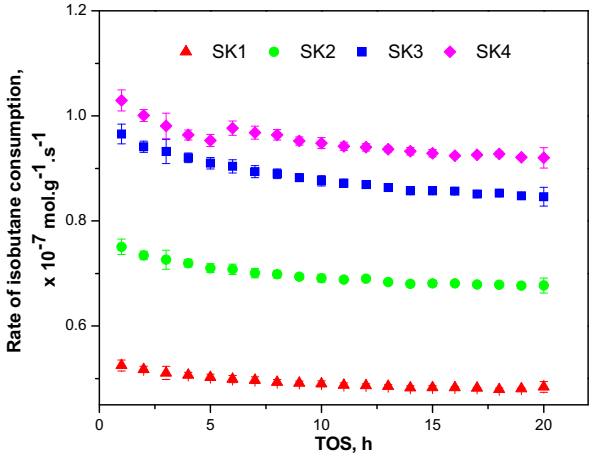

Fig. 6. Rate of isobutane consumption versus time-on-stream (TOS). Reaction conditions: $P_{i\text{-}C_4H_{10}} = 2.02$ kPa, $P_{O_2} = 1.0$ kPa, $T = 400$ °C, catalyst weight: 200 mg.

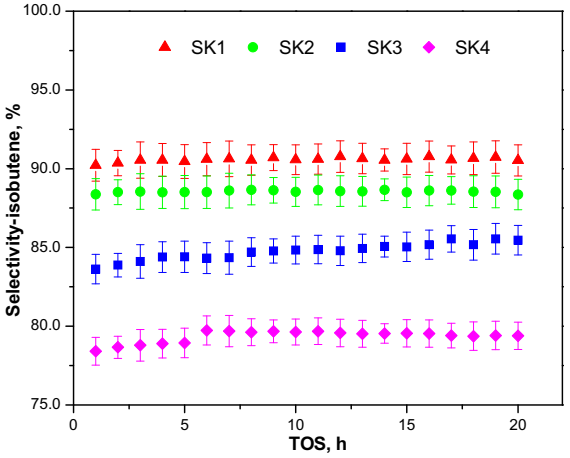

Fig. 7. Isobutene selectivity versus time-on-stream (TOS). Reaction conditions: $P_{i\text{-}C_4H_{10}} = 2.02$ kPa, $P_{O_2} = 1.01$ kPa, $T = 400$ °C, catalyst weight: 200 mg.

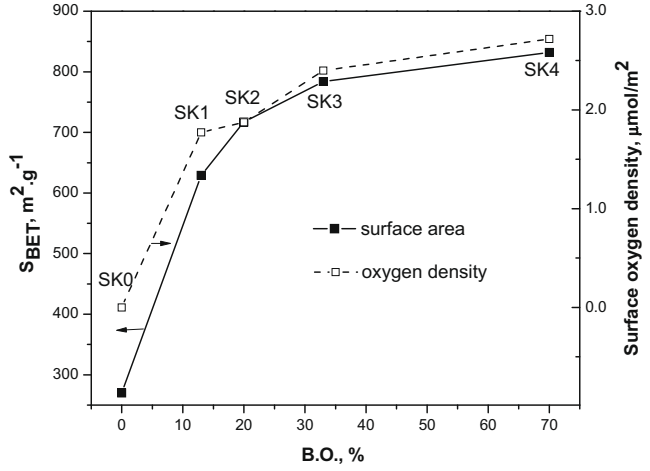

Fig. 8a. Surface area and oxygen density as a function of B.O. for GMCs. The density of oxygen sites was calculated taking into account the total amount of oxygen desorbed during TPD (Table 2) and the total surface area of each carbon (Table 1).

isobutene is a dehydrogenated intermediate product that can either desorb as isobutene from carbon surface or be captured by neighboring dissociated oxygen species to form CO or CO_2.

The progressive changes in the ratio of edge to basal-planes and the amount of surface oxygen groups deposited on the surface due to the systematic burn-off process clearly causes changes in activity and selectivity. The effect of burn-off on the surface chemistry of the carbons and their catalytic performance are given in Fig. 8 and Table 3. Fig. 8a shows how both the surface area and oxygen density systematically varied by increasing the burn-off, whereas Fig. 8b shows the changes in activity and selectivity with burn-off. Table 3 presents the isobutane steady-state rate (defined at 15 h TOS) normalized on the basis of catalyst weight, total surface area, and total oxygen content. It can be clearly observed that isobutane conversion, specific rate, and areal rate increase with burn-off. However, there is a 1.9-fold increase of conversion and specific rate from the lower burn-off catalyst (SK1) to the highest burn-off catalyst (SK4), whereas the areal rate only presents a 1.45-fold increase. It is important to emphasize that areal rate is based on the total surface area, which includes both the inactive basal-planes and the catalytic active edge planes. The isobutane consumption normalized by oxygen content increases for the first two samples and then decreases as the burn-off progresses. The small variation of the rate with oxygen content could indicate that the total oxygen content measured by TPD would be a proper basis for calculation of turnover rates. However, care should be taken as there are most likely uncovered edge sites that can originate a different type of active site. Indeed, it is well-known that not only the oxygen functionality, but the defect edge sites of graphitic carbons contain various active sites such as arm-chair and zig-zag sites with different reactivities that can create sites for different oxygen species. For instance, arm-chair sites have been reported to be less active

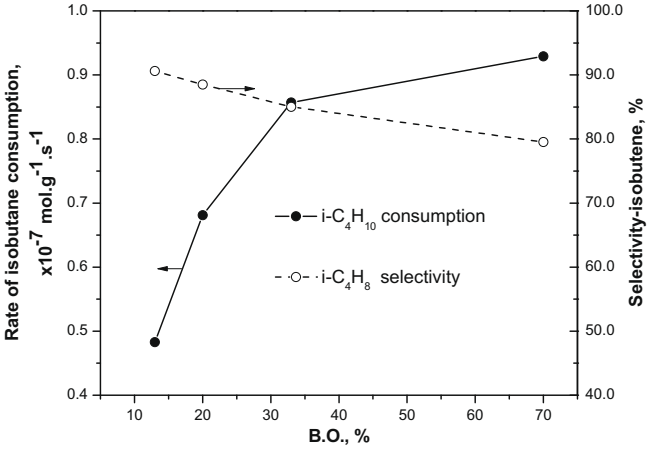

Fig. 8b. Isobutane consumption rate and isobutene selectivity after 15 h time-on-stream (TOS). Reaction conditions: $P_{i\text{-}C_4H_{10}} = 2.02$ kPa, $P_{O_2} = 1.01$ kPa, $T = 400$ °C, catalyst weight: 200 mg.

than zig-zag ones [18]. Therefore, a more detailed analysis of reaction pathways and kinetics is necessary in order to draw conclusions about the selective active sites for ODH reaction to see whether they are related to the oxygen functionalities deposited on the carbon edge surface or the dissociatively adsorbed O created on the open edges and defect sites during reaction.

Oxidative dehydrogenation reaction of alkanes have been extensively studied over oxide catalysts [1,3,8,9] and the reaction sequence has been mostly described to involve parallel-consecutive steps as illustrated for the case of ODH of isobutane in Scheme

Table 3
Conversion and reaction rates at steady-state (15 h TOS).

GMC catalyst	Conversion[a] (%)	Specific rate[b] (mol g^{-1} s^{-1})	Areal rate[c] (mol m^{-2} s^{-1})	Normalized rate[d] (s^{-1})
SK1	1.8	4.83E−08	7.68E−11	4.33E−05
SK2	2.5	6.81E−08	9.50E−11	5.07E−05
SK3	3.2	8.57E−08	1.09E−10	4.55E−05
SK4	3.4	9.29E−08	1.12E−10	4.11E−05

[a] Conversion: based on isobutane conversion.
[b] Specific rate: based on isobutane consumption.
[c] Areal rate: based on BET surface area.
[d] Normalized Rate: based on the total oxygen content.

1. In this scheme, isobutene is a primary product of the oxidative dehydrogenation whereas carbon oxides can form via either subsequent oxidation of isobutene or direct catalytic combustion of isobutane. This sequence is believed to occur also in carbon-based catalysts during ODH of *n*-butane [6]. In order to verify the reaction network occurring in our GMCs, a simple method based on an analysis of selectivity-conversion was carried out [9,24]. Primary products of a reaction can be discriminated from secondary or even higher-order products by checking the zero-conversion intercept of their selectivities. In this method, products with non-zero intercepts are from the primary reactions.

Fig. 9 shows the selectivity-conversion plot for the SK2 catalyst measured at 400 °C with an oxygen:isobutane ratio of 1:2. The selectivity to isobutene increased when isobutane conversion decreased but did not reach 100% when extrapolated to zero conversion. Selectivity analyses of CO and CO_2 confirmed that both species were also primary products of ODH of isobutene, as non-zero intercepts were found for the selectivities at zero conversion. Similar trends were also observed for the other carbons, SK1, SK3, and SK4 (not shown), which further confirmed a parallel-consecutive reaction network.

The presence of two parallel-consecutive pathways is of particular interest as it suggests the existence of different surface sites, responsible for the partial oxidation or deep oxidation products, separately. Indeed, the involvement of distinct forms of reactive oxygen species has been investigated especially in the case of oxide catalysts [2,25]. In that case, it is generally believed that lattice oxygen sites could be responsible for the partial oxidation following a Mars–Van Krevelen (MVK) type of mechanism whereas the deep oxidation could be carried out over the dissociatively adsorbed oxygen species following a Langmuir–Hinshelwood (LH) mechanism. However, little is known regarding the oxygen active sites of carbon-based catalysts [26]. Most of the studies so far have been carried out using complex activated carbons as catalysts for ODH of ethylbenzene [19,27,28]. These studies suggest that the activity increases with the degree of oxidation and that the quinone/carbonyl functional groups are the active sites for such reaction. In more recent work, Zhang et al. [6] examined the ODH reaction of butane on carbon nanotubes and, likewise, demonstrated the same parallel-consecutive pathway as we observed. Previously [7], we reported that the open edges of the fullerene-like cavities are crucial for the catalytic activity of our highly stable GMCs. If indeed the partial oxidation takes place over an oxygen functional group, the formation rate of isobutene should present a zero-order dependence on the O_2 partial pressure P_{O_2} as in a MVK-type mechanism. Fig. 10 shows the rate dependence for the SK2 catalyst. As opposed to a zero-order dependence on P_{O_2}, we found that isobutene formation rate increased with P_{O_2} and the dependence could be fitted using a reaction order of 0.22 in P_{O_2}. Partial order dependence is a strong indication that dissociative adsorption of O_2 is a step of the reaction mechanism leading to the partial oxidation product.

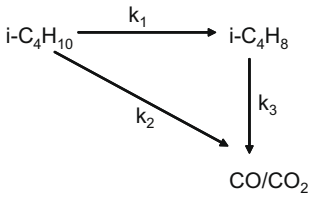

Scheme 1. Reaction network in oxidative dehydrogenation of isobutane.

3.3. Reaction rates: a selectivity study

A more detailed kinetic analysis can be performed by variation of reactants flow and working at differential conversions. Following the method described by Khodakov et al. [3], reaction rate and selectivity for isobutene can be extrapolated to zero conversion in order to determine the relative rates of the primary dehydrogenation and the parallel-consecutive oxidation reactions. This method is based on assuming a first-order kinetic analysis of the network and treating the concentrations of isobutane and oxygen as constant at low conversion levels. The rates of each pathway shown in Scheme 1 can be then simplified as follows:

$$r_1 = k_1' P_{i\text{-}C_4H_{10}}^{\alpha_1} P_{O_2}^{\beta_1} = k_1 P_{i\text{-}C_4H_{10}}, \quad (1)$$

$$r_2 = k_2' P_{i\text{-}C_4H_{10}}^{\alpha_2} P_{O_2}^{\beta_2} = k_2 P_{i\text{-}C_4H_{10}}, \quad (2)$$

$$r_3 = k_3' P_{i\text{-}C_4H_8}^{\alpha_3} P_{O_2}^{\beta_3} = k_3 P_{i\text{-}C_4H_8}, \quad (3)$$

where r_n is the reaction rate per gram of carbon and k_n is the first-order rate coefficient for reaction n, $n = 1, 2, 3$.

The rate for isobutene formation can be written for a differential weight (dW) and total volumetric rate (F) as

$$\frac{F}{RT}\frac{dP_{i\text{-}C_4H_8}}{dW} = k_1 P_{i\text{-}C_4H_{10}} - k_3 P_{i\text{-}C_4H_8}. \quad (4)$$

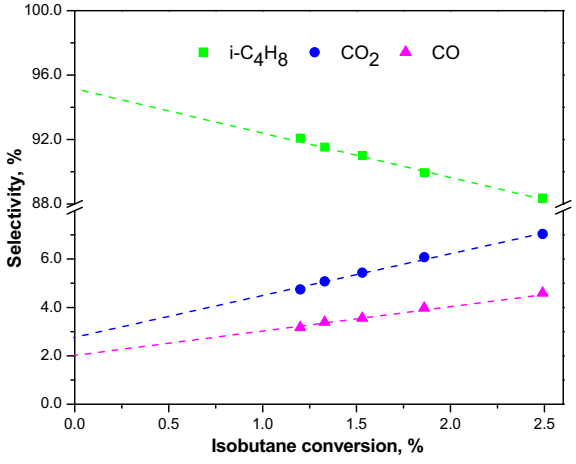

Fig. 9. Isobutene, CO, and CO_2 selectivity profiles in ODH of isobutane over SK2 catalyst at 400 °C, $P_{i\text{-}C_4H_{10}}$:P_{O_2} = 2 : 1, catalyst weight: 200 mg.

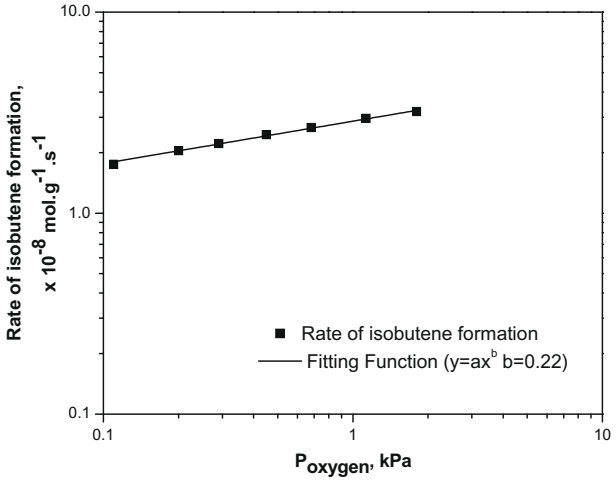

Fig. 10. Isobutene formation rate as a function of P_{O_2} over SK2 catalyst, reaction conditions: T = 400 °C $P_{i\text{-}C_4H_{10}}$ = 0.45 kPa, catalyst weight: 200 mg.

Fig. 11a shows the experimental dependence between the rate of isobutene formation and weight time (W/F). From the model described by Khodakov et al. [3], it can be shown that at small W/F, the rate can be expanded as a quadratic dependence upon W/F. The value of k_1 can be obtained from quadratic extrapolation for W/F approaching zero (zero conversion) as shown in Fig. 11a. In this case, k_1 is calculated from

$$k_1 = \frac{r_{(W/F=0)}}{P^0_{i\text{-}C_4H_{10}}}, \tag{5}$$

where $r_{(W/F=0)}$ is the extrapolated rate as W/F goes to zero and $P^0_{i\text{-}C_4H_{10}}$ is the initial partial pressure of isobutane.

Following the same methodology described by Khodakov et al. [3], isobutene selectivity can be expressed by Eq. (6), as a linear function of W/F.

$$S_{i\text{-}C_4H_8} = \frac{k_1}{k_1+k_2} - \left(\frac{k_1}{k_1+k_2}\right)\frac{k_1+k_2+k_3}{2}RT\frac{W}{F}. \tag{6}$$

Fig. 11b shows the linear fit of our experimental selectivity for isobutene at variable weight time. Once k_1 is known from the above-mentioned equation, the rate constant k_2 can be calculated by the intercept of isobutene selectivity at zero weight time, which is $\frac{k_1}{k_1+k_2}$. Then k_3 can be calculated from the slope of the fitted line as expressed by Eq. (6). The computed values of the three rate constants are given in Fig. 12 for all the functionalized GMC carbons.

The calculated reaction rate constants were plotted as a function of surface oxygen (Fig. 12). The rate constant leading to the partial oxidation product does not show a strong correlation to the density of the oxygen sites and, indeed, it remains fairly constant above a certain level. On the other hand, the rate constant leading to the total combustion increases continuously with the density of oxygen sites. These differences appear to suggest that the two reactions take place on different sites. However, different from reported elsewhere [5,6,19,20], quinone-type functional groups show only correlation to the total combustion pathway. Additionally, the direct combustion pathway should play a less important role since rate constant analyses show that CO_x were formed mainly by the consecutive deep oxidation of isobutene.

It is still very hard to decouple the effect of the oxygen functional sites to the number of defect edge sites. The air treatment process utilized to create the oxygen sites on the mesoporous carbon surface was also responsible for the opening of the fullerene-like cavities and the exposition of the edge sites. Evidently, more than one type of sites are involved in the different pathways, which is not surprising giving that others [29,30] have shown that on oxide catalysts, the partial oxidation pathway is structure insensitive and the total combustion is structure sensitive. Our studies indicate that our highly stable GMCs modified by mild oxidation suppress the direct total combustion pathway and, that, no clear correlation was observed between the quinone-type functional sites and the selective oxidation products.

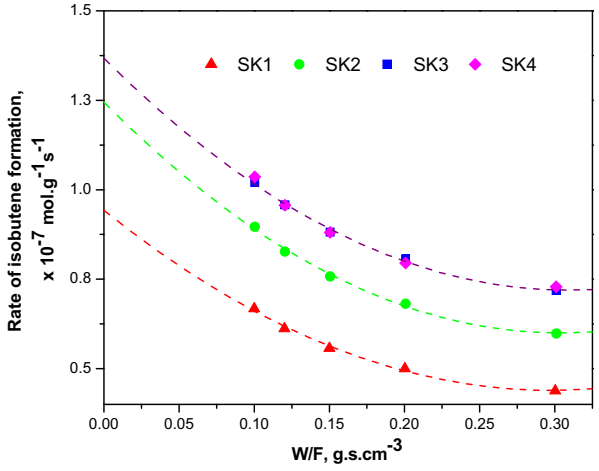

Fig. 11a. Rate of isobutene formation as a function of W/F: $P_{i\text{-}C_4H_{10}} = 2.02$ kPa, $P_{O_2} = 1.01$ kPa, catalyst weight = 200 mg. Conversions in all cases are less than 4%.

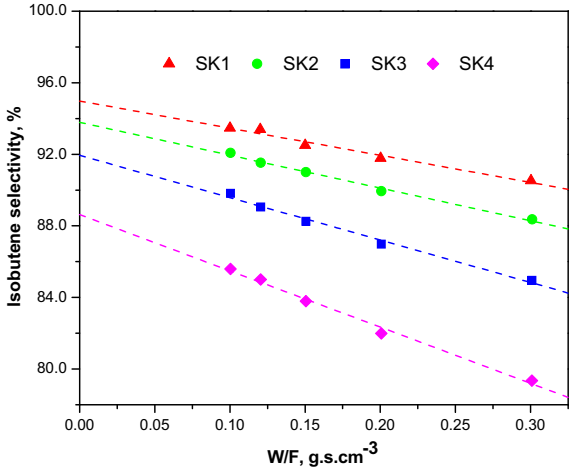

Fig. 11b. Isobutene selectivity as a function of W/F:$P_{i\text{-}C_4H_{10}} = 2.02$ kPa, $P_{O_2} = 1.01$ kPa, catalyst weight = 200 mg. Conversions in all cases are less than 4%.

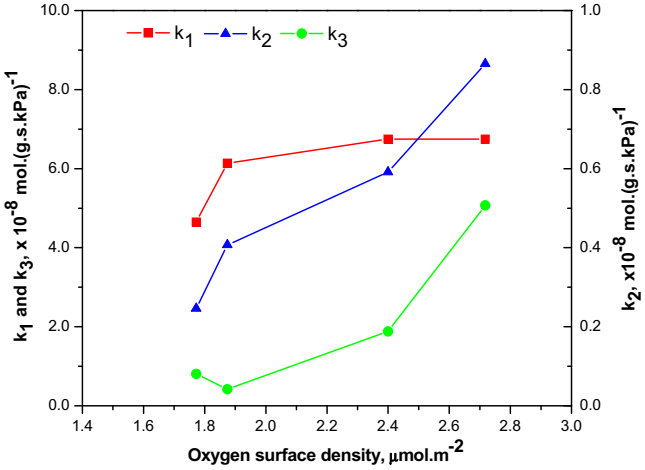

Fig. 12. Dependence of the calculated rate constants of k_1, k_2, and k_3, assuming a first-order analysis, on the density of surface oxygen for different carbons.

4. Conclusions

In this study, we demonstrated that the controlled air oxidation is a facile method for the preparation of model carbon catalysts that contain a tunable amount of quinone-type oxygen functionality on the surface of GMCs. The concentration of the oxygenated functional groups on the surface of the GMCs is tunable in a continuous manner through a simple control of the burn-off level. Systematically varying the concentration of the oxygenated functional groups opens an avenue to investigate the function of oxygenated functional groups in the ODH reactions with least influence from the complexity of traditional carbon materials which vary in composition of surface functional groups, the impu-

rity of minerals, the sp^2 and sp^3 hybridization carbon atoms structure, and porous structures. Kinetic studies using these GMC catalysts show the concurrence of a consecutive pathway for the partial oxidative dehydrogenation for the formation of isobutene and subsequent CO and CO_2, and a parallel deep oxidation pathway for direct formation of CO and CO_2 from isobutane. Initial rate constant analyses suggest that two different active sites appear to be responsible for partial oxidative dehydrogenation and deep oxidation processes separately. No clear correlation was observed between the quinone-type functional sites and the selective oxidation product, which is different from the current commonly accepted concept that only the surface oxygen-containing groups are responsible for the ODH reactions on carbon catalysts. Given the complexity of the carbon surface, although these model catalysts have a simple surface structure, the edge planes are not completely covered by the oxygenated functionalities. The possible involvement of the uncovered edge sites and defect sites in the ODH reaction yields to uncertainties in probing the origin of the selectivity of carbon catalysts for ODH reactions; further identification of the uncovered edge sites and defects on the carbon catalysts may lead to a thorough understanding of the ODH reaction mechanism and therefore enables the rational design of catalysts with desirable properties.

Acknowledgments

This research was supported by the Center for Nanophase Materials Sciences, which is sponsored at Oak Ridge National Laboratory by the Scientific User Facilities Division, Office of Basic Energy Sciences, U.S. Department of Energy. The research was supported in part by an appointment to the ORNL Postdoctoral Research Associates Program administered jointly by Oak Ridge Institute for Science and Education (ORISE) and ORNL. James W. Klett and Jim Kiggans at ORNL are gratefully acknowledged for their assistance with the graphitization process.

References

[1] Y.A. Agafonov, N.V. Nekrasov, N.A. Gaidai, A.L. Lapidus, Kinet. Catal. 48 (2007) 255–264.
[2] J.N. Michaels, D.L. Stern, R.K. Grasselli, Catal. Lett. 42 (1996) 139–148.
[3] A. Khodakov, J. Yang, S. Su, E. Iglesia, A.T. Bell, J. Catal. 177 (1998) 343–351.
[4] J.J. Delgado, D.S. Su, G. Rebmann, N. Keller, A. Gajovic, R. Schlogl, J. Catal. 244 (2006) 126–129.
[5] J.D.D. Velasquez, L.A.C. Suarez, J.L. Figueiredo, Appl. Catal. A – Gen. 311 (2006) 51–57.
[6] J. Zhang, X. Liu, R. Blume, A.H. Zhang, R. Schlogl, D.S. Su, Science 322 (2008) 73–77.
[7] C.D. Liang, H. Xie, V. Schwartz, J. Howe, S. Dai, S.H. Overbury, J. Am. Chem. Soc. 131 (2009) 7735–7741.
[8] S. Albonetti, F. Cavani, F. Trifiro, Catal. Rev. – Sci. Eng. 38 (1996) 413–438.
[9] J.N. Michaels, D.L. Stern, R.K. Grasselli, Catal. Lett. 42 (1996) 135–137.
[10] C.D. Liang, S. Dai, J. Am. Chem. Soc. 128 (2006) 5316–5317.
[11] F. Tuinstra, J.L. Koenig, J. Chem. Phys. 53 (1970) 1126.
[12] A.C. Ferrari, J. Robertson, Phys. Rev. B 61 (2000) 14095–14107.
[13] C.D. Liang, Z.J. Li, S. Dai, Angew. Chem., Int. Ed. 47 (2008) 3696–3717.
[14] S. Lowell, J. Shields, M. Thomas, TM, Characterization of Porous Solids and Powders: Surface Area, Pore size, and Density, Springer, Netherland, 2004. 347p.
[15] M. Steinhart, C.D. Liang, G.W. Lynn, U. Gosele, S. Dai, Chem. Mater. 19 (2007) 2383–2385.
[16] U. Zielke, K.J. Huttinger, W.P. Hoffman, Carbon 34 (1996) 983–998.
[17] B. Marchon, W.T. Tysoe, J. Carrazza, H. Heinemann, G.A. Somorjai, J. Phys. Chem. 92 (1988) 5744–5749.
[18] S.E. Stein, R.L. Brown, Carbon 23 (1985) 105–109.
[19] M.F.R. Pereira, J.J.M. Orfao, J.L. Figueiredo, Appl. Catal. A – Gen. 184 (1999) 153–160.
[20] J.L. Figueiredo, M.F.R. Pereira, M.M.A. Freitas, J.J.M. Orfao, Carbon 37 (1999) 1379–1389.
[21] V. Strelko, D.J. Malik, M. Streat, Carbon 40 (2002) 95–104.
[22] G.W. Roberts, C.N. Satterfield, Indus. Eng. Chem. Fundam. 4 (1965) 288–293.
[23] A. Dufour, A. Celzard, B. Ouartassi, F. Broust, V. Fierro, A. Zoulaljan, Appl. Catal. A – Gen. 360 (2009) 120–125.
[24] N.A. Bhore, M.T. Klein, K.B. Bischoff, Ind. Eng. Chem. Res. 29 (1990) 313–316.
[25] R. Grabowski, Catal. Rev. 48 (2006) 199–268.
[26] F. Rodriguez-Reinoso, Carbon 36 (1997) 159–175.
[27] A. Guerreroruiz, I. Rodriguezramos, Carbon 32 (1994) 23–29.
[28] M.F.R. Pereira, J.J.M. Orfao, J.L. Figueiredo, Colloids Surf. A – Physicochem. Eng. Aspects 241 (2004) 165–171.
[29] S.T. Oyama, J. Catal. 128 (1991) 210–217.
[30] A. Baiker, D. Monti, J. Catal. 91 (1985) 361–365.